Prediction of Shrinkage Pore Volume Fraction Using a Dimensionless Niyama Criterion

KENT D. CARLSON and CHRISTOPH BECKERMANN

A method is presented to use a dimensionless form of the well-known Niyama criterion to directly predict the amount of shrinkage porosity that forms during solidification of metal alloy castings. The main advancement offered by this method is that it avoids the need to know the threshold Niyama value below which shrinkage porosity forms; such threshold values are generally unknown and alloy dependent. The dimensionless criterion accounts for both the local thermal conditions (as in the original Niyama criterion) and the properties and solidification characteristics of the alloy. Once a dimensionless Niyama criterion value is obtained from casting simulation results, the corresponding shrinkage pore volume fraction can be determined knowing only the solid fraction-temperature curve and the total solidification shrinkage of the alloy. Curves providing the shrinkage pore volume percentage as a function of the dimensionless Niyama criterion are given for WCB steel, aluminum alloy A356, and magnesium alloy AZ91D. The present method is used in a general-purpose casting simulation software package to predict shrinkage porosity in three-dimensional (3-D) castings. Comparisons between simulated and experimental shrinkage porosity results for a WCB steel plate casting demonstrate that this method can reasonably predict shrinkage. Additional simulations for magnesium alloy AZ91D illustrate that this method is applicable to a wide variety of alloys and casting conditions.

DOI: 10.1007/s11661-008-9715-y

I. INTRODUCTION

THE Niyama criterion[1] is presently the most widely used criterion function in metal casting. It is used to predict feeding-related shrinkage porosity caused by shallow temperature gradients. All casting simulation software packages calculate the Niyama criterion as a standard output; foundries worldwide use this criterion to predict the presence of shrinkage in castings. Foundry-simulation users view Niyama contour plots predicted by a casting simulation and expect that shrinkage porosity will form in regions that contain Niyama values below some threshold value. The Niyama criterion is a local thermal parameter defined as

$$Ny = G\Big/\sqrt{\dot{T}} \qquad [1]$$

where G is the temperature gradient and $\dot{T}$ is the cooling rate, both of which are evaluated at a specified temperature near the end of solidification. Niyama *et al.*[1] empirically determined the functional form of this criterion, but they also offered a physical model as justification. The model begins with Darcy's law, which relates the interdendritic feeding-flow velocity to the pressure drop across the mushy zone. By making simplifying assumptions about the functional form of the solid fraction-temperature curve and the permeability, they were able to analytically integrate the one-dimensional (1-D) form of Darcy's law to demonstrate that $\Delta P \propto \dot{T}/G^2$ (or $\Delta P \propto Ny^{-2}$), where ΔP is the pressure drop across the mushy zone. By comparing experimentally observed shrinkage porosity patterns in cast-steel cylinders to corresponding casting simulations, Niyama *et al.* discovered that there was a threshold value of Ny below which shrinkage was typically present. While the presence of the temperature gradient in Eq. [1] is not surprising, and implies that shrinkage porosity will form in regions of low G, the presence of the cooling rate (albeit inside a square root) in the denominator may at first seem counterintuitive. The Niyama criterion predicts that shrinkage porosity increases with increasing cooling rate, because the feeding-flow velocities and the resulting pressure drop across the mushy zone are higher for higher solidification rates. It follows that the beneficial effect of a chill, for example, is due to the increase in the temperature gradient the chill provides; the concomitant increase in the cooling rate near a chill is actually counterproductive with regard to avoiding shrinkage porosity.

To illustrate the correlation between low Niyama values and shrinkage porosity, a sample Niyama result, based on experiments conducted in a previous study,[2] is given for the end-risered plate 1 × 5.5 × 19 in. (25.4 × 140 × 483 mm) in size shown schematically in Figure 1(a). Fifteen such plates were cast from WCB steel (Table I) in a sand mold (five plates each by three different foundries). The plates were then radiographed (sample radiographs are shown in Figures 1(b) and (c)), and the shrinkage evident on the radiographs was

KENT D. CARLSON, Research Engineer, and CHRISTOPH BECKERMANN, Professor, are with the Department of Mechanical and Industrial Engineering, The University of Iowa, Iowa City, IA 52242. Contact e-mail: becker@engineering.uiowa.edu
Manuscript submitted July 28, 2008.
Article published online November 26, 2008

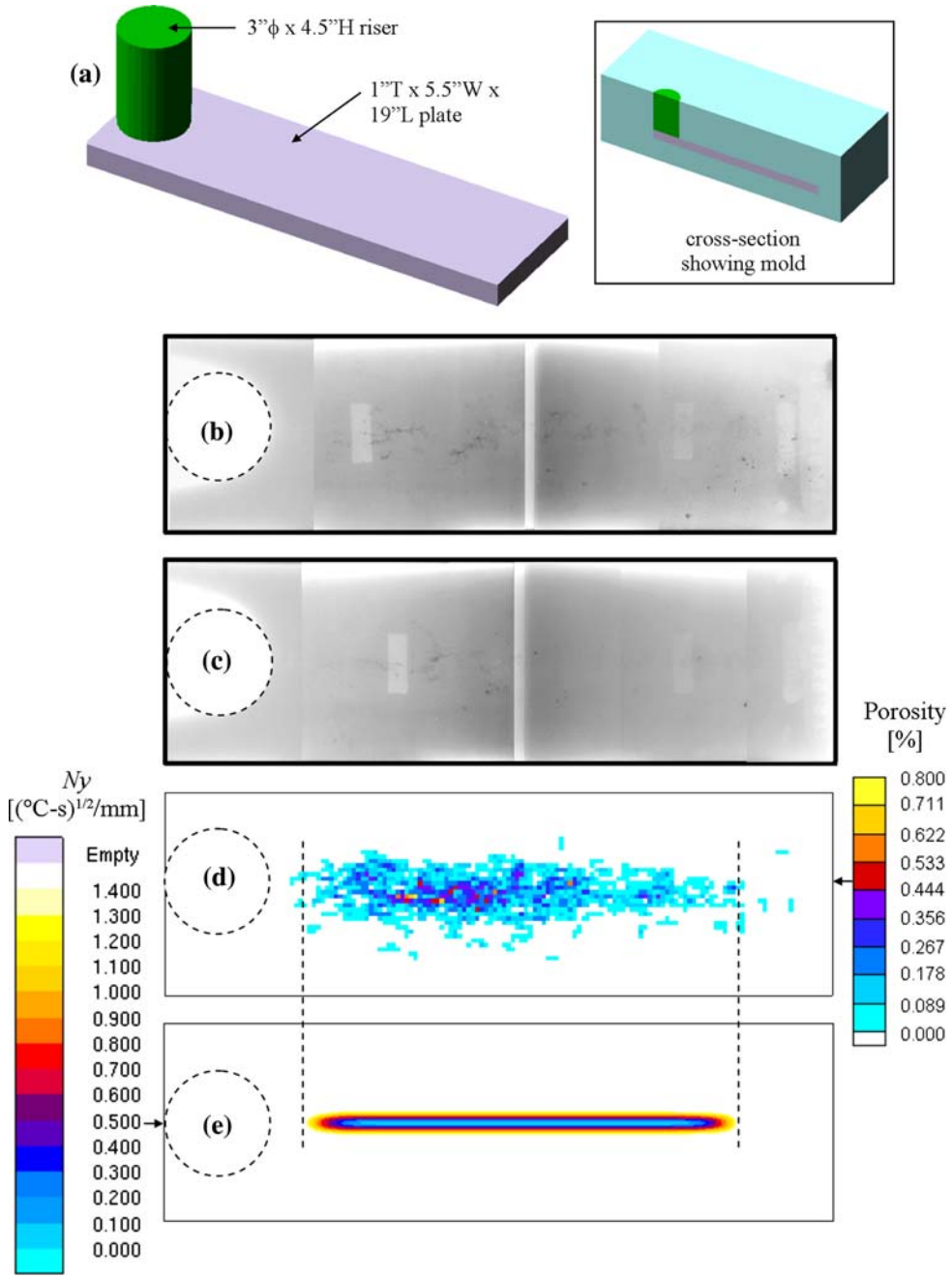

Fig. 1—Comparison between experimental shrinkage porosity and Niyama criterion predictions for WCB steel plates: (*a*) schematic of the plate and riser; (*b*) and (*c*) radiographs of two plates; (*d*) average through-thickness porosity of 15 plates; and (*e*) predicted Niyama criterion distribution at the plate midplane.

Table I. Compositions for the Alloys of Interest, Given in Weight Percent

	Composition (Wt Pct)											
Alloy	Al	C	Cr	Cu	Fe	Mg	Mn	P	S	Si	Ti	Zn
WCB	—	0.19	0.2	—	bal	—	1.25	0.04	0.045	0.4	—	—
A356	bal	—	—	0.01	0.1	0.37	0.01	—	—	7.0	0.08	0.01
AZ91D	8.61	—	—	0.003	0.0038	bal	0.23	—	—	0.017	—	0.6

digitized by overlaying a 1-mm-square grid on top of each radiograph and visually determining for each square whether shrinkage was present. If shrinkage was present, it was assumed to be 100 pct shrinkage for 1 mm in depth, thus providing an estimate of the through-thickness shrinkage porosity. The shrinkage from the 15 digitized radiographs was then averaged, giving the composite through-thickness porosity result shown in Figure 1(d). The corresponding midthickness-plane Niyama plot from a casting simulation of these plates is shown in Figure 1(e). Note that the region of low Niyama values is in good qualitative agreement with the region containing the bulk of the significant centerline shrinkage porosity in the experimental result in Figure 1(d). The low-Niyama region is not as wide as the shrinkage-containing region seen experimentally, but the length of the shrinkage-containing region is predicted quite well.

Foundries use the Niyama criterion primarily in a qualitative fashion, to identify regions in a casting that are likely to contain shrinkage porosity. The reason for such limited use is twofold: (1) the threshold Niyama value below which shrinkage porosity forms is generally unknown, other than for steel, and can be quite sensitive to the type of alloy being cast and sometimes even to the casting conditions (*e.g.*, sand mold *vs* steel mold, application of pressure, *etc.*); and (2) the Niyama criterion does not provide the actual amount of shrinkage porosity that forms, other than in a qualitative fashion (*i.e.*, the lower the Niyama value, the more shrinkage porosity forms). Threshold Niyama values reported in the literature depend on the sensitivity of the method with which the presence or absence of shrinkage porosity was determined. For example, Niyama *et al.*[1] and Carlson *et al.*[2] relied on the visual rating of radiographs of limited sensitivity to establish a threshold Niyama value for steel sand castings. In another study involving steel castings, Carlson *et al.*[3] found that, in order to predict microshrinkage that is not detectable using radiography, a much higher threshold Niyama value should be used.

There is no reason to use the Niyama criterion only for steel castings. It can also be expected to predict shrinkage porosity in other alloys, such as those based on Ni, Mg, or Al. Carlson *et al.*[4] determined a threshold Niyama value for Ni-alloy sand castings that is higher than the one found earlier for steel. Shrinkage porosity is also a widespread problem in Mg-alloy castings, and at least one study has been performed in which the Niyama criterion was found to correlate qualitatively well with porosity measurements for Mg-alloy castings.[5] For Al-alloy castings, hydrogen-related gas porosity is often a major factor,[6,7] but if the Al alloy is well degassed, shrinkage porosity can also be a problem.[7] However, threshold Niyama criterion values for Mg and Al alloys have not been established. Because the Niyama criterion is only a function of thermal parameters and does not take into account the properties and solidification characteristics of an alloy, it is not universal in nature; calculated Niyama criterion values for one alloy do not mean the same as those for another alloy.

The purpose of the present investigation is to develop a criterion function that can be used to predict not only the presence of shrinkage porosity in castings but also the quantity of shrinkage that forms. The ability to predict actual shrinkage pore volume fractions (or percentages) completely avoids the need to know threshold values. The criterion function developed here is a dimensionless version of the Niyama criterion that accounts for not only the thermal parameters but also the properties and the solidification characteristics of the alloy. Once the dimensionless Niyama criterion is presented, it is shown how it can be used to predict the shrinkage pore volume fraction knowing only the solid fraction-temperature curve and the total solidification shrinkage of the alloy. Parametric studies are performed to investigate the effects of the pressure and cooling rate on the resulting pore volume. The new criterion is then applied in several three-dimensional (3-D) casting simulations, to illustrate its utility. It is emphasized that the present study is not intended to provide additional experimental verification of the validity of the Niyama criterion in general, because such validation is already available.[1–5,7,8]

II. MODEL DEVELOPMENT

The present criterion is derived for the directionally solidifying 1-D system shown schematically in Figure 2. Darcy's law can be written for this system as

$$g_l u_l = -\frac{K}{\mu_l}\frac{\mathrm{d}P}{\mathrm{d}x} \qquad [2]$$

where g_l is the liquid volume fraction, u_l is the liquid velocity in the mushy zone (*i.e.*, shrinkage velocity), μ_l is the liquid dynamic viscosity, P is the melt pressure, and x is the spatial coordinate, as indicated in Figure 2. The permeability in the mushy zone, K, is determined from the Kozeny–Carman relation

$$K = K_0 \frac{g_l^3}{(1-g_l)^2} \qquad [3]$$

where, as a first approximation, $K_0 = \lambda_2^2/180$, in which λ_2 is the secondary dendrite arm spacing (SDAS).

Assuming that the liquid and solid densities (ρ_s and ρ_l) are constant during solidification, one can define the total solidification shrinkage in terms of these densities as $\beta = (\rho_s - \rho_l)/\rho_l$. Using β to simplify the 1-D mass conservation equation and then integrating the result, it can be shown that the shrinkage velocity throughout the mushy zone is constant and can be expressed as $u_l = -\beta R$, where R is the constant isotherm velocity (Figure 2). If one further realizes that R can be expressed in terms of the temperature gradient, G ($= \mathrm{d}T/\mathrm{d}x$), and the cooling rate, $\dot{T}$ ($= \mathrm{d}T/\mathrm{d}t$), the shrinkage velocity in the mushy zone can be written as

$$u_l = -\beta R = -\beta \dot{T}/G \qquad [4]$$

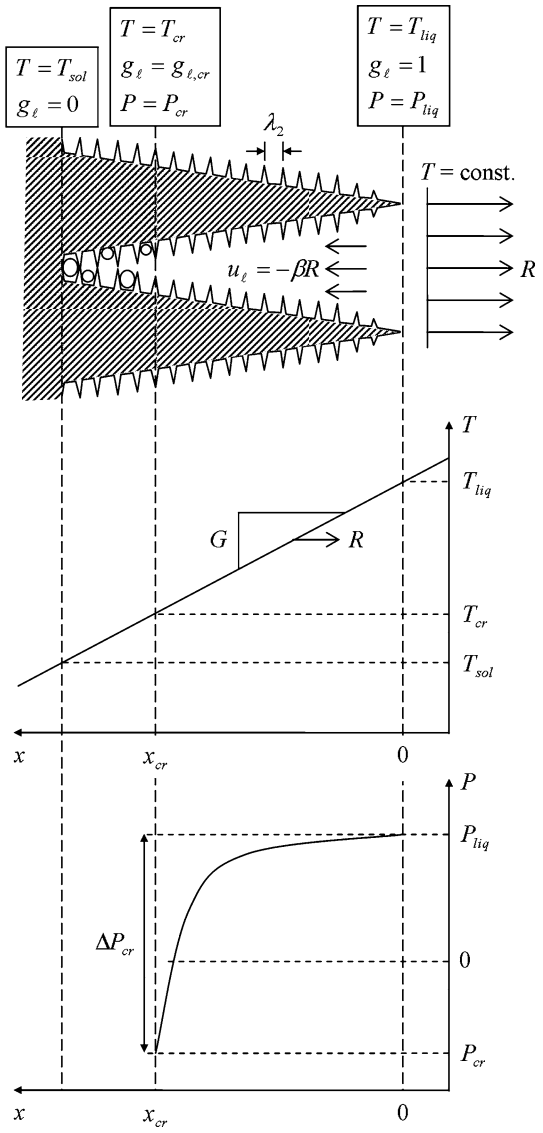

Fig. 2—Schematic of a 1-D mushy zone solidifying with constant temperature gradient, G, and isotherm velocity, R.

Substituting this expression into Eq. [2] yields

$$\frac{\mathrm{d}P}{\mathrm{d}x} = \frac{\mu_l \beta \dot{T} g_l}{KG} \qquad [5]$$

Figure 2 illustrates that, as the solid fraction increases, the melt pressure decreases from the value at the liquidus, P_{liq}, down to some critical pressure, P_{cr}, at which point shrinkage porosity begins to form. For convenience, the critical pressure drop can be defined as $\Delta P_{cr} = P_{\mathrm{liq}} - P_{cr}$. The pressure at liquidus is simply the sum of the ambient pressure of the system and the local head pressure. The critical pressure is determined by considering the mechanical equilibrium necessary for a stable pore to exist. This equilibrium is given by the Young–Laplace equation as $P_{cr} = P_p - P_\sigma$, where P_p is the pressure inside the pore and P_σ is the capillary pressure. The capillary pressure is given by $P_\sigma = 2\sigma/r_0$, where σ is the surface tension between the pore and the surrounding liquid and r_0 is the initial radius of curvature at pore formation. For pure shrinkage, in the absence of dissolved gases in the melt, the pressure inside the pores is negligibly small (due only to the vapor pressure of the elements in the melt). With this, the Young–Laplace equation simplifies to

$$P_{cr} = -P_\sigma = -\frac{2\sigma}{r_0} \qquad [6]$$

Note that Eq. [6] implies that the critical pressure is a negative number; this is reasonable, because the surface tension must be overcome before porosity can form. Generally, the capillary pressure at pore formation, P_σ, is an unknown quantity, primarily because the initial radius of curvature of the pores is unknown. Shrinkage pores typically nucleate heterogeneously from pre-existing bubbles associated with oxides, other inclusions, and small cavities in mold walls. The radius of curvature when porosity forms is a function of the nature, size, and geometry of the nucleation sites, which in turn is influenced by melt quality. In the following, ΔP_{cr} is simply treated as an adjustable parameter, and the effect of varying ΔP_{cr} is investigated in detail. Clearly, the uncertainty in P_σ overshadows any inaccuracies in P_p or small changes in P_{liq}, due to varying metallostatic head.

The point in space at which shrinkage porosity begins to form can be determined by integrating Eq. [5] over the mushy zone from the critical point to the liquidus, assuming that the viscosity, temperature gradient, and cooling rate are constant over the interval being considered:

$$\int_{P_{cr}}^{P_{\mathrm{liq}}} \mathrm{d}P = \Delta P_{cr} = \int_{x_{cr}}^{0} \frac{\mu_l \beta \dot{T} g_l}{KG} \mathrm{d}x = \int_{T_{cr}}^{T_{\mathrm{liq}}} \frac{\mu_l \beta \dot{T} g_l}{KG} \frac{\mathrm{d}x}{\mathrm{d}T} \mathrm{d}T = \frac{\mu_l \beta \dot{T}}{G^2} \int_{g_{l,cr}}^{1} \frac{g_l}{K} \frac{\mathrm{d}\dot{T}}{\mathrm{d}g_l} \mathrm{d}g_l \qquad [7]$$

where x_{cr}, T_{cr}, and $g_{l,cr}$ are the position, temperature, and liquid fraction, respectively, at which the melt pressure drops to P_{cr} and porosity begins to form (Figure 2). Equation [7] is essentially the same expression that was derived by Niyama *et al.*,[1] Lee *et al.*,[9] Sigworth and Wang,[6] and Dantzig and Rappaz.[10] Subsequent differences in their resulting criteria (as well as in the present criterion) stem from assumptions made regarding the solid fraction-temperature curve ($g_s(T)$, where $g_s = 1 - g_l$) and the permeability in the integral in Eq. [7], as well as the manner in which the result is cast and used.

In order to nondimensionalize the final integral in Eq. [7], one can introduce a dimensionless temperature, $\theta = (T - T_{\mathrm{sol}})/\Delta T_f$, where $\Delta T_f = T_{\mathrm{liq}} - T_{\mathrm{sol}}$ is the freezing range, T_{liq} is the liquidus temperature, and T_{sol} is the temperature at which the alloy is 100 pct solidified. Introducing this expression along with Eq. [3] into Eq. [7] yields

$$\Delta P_{cr} = \frac{\mu_l \beta \Delta T_f}{\lambda_2^2} \frac{\dot{T}}{G^2} I(g_{l,cr}) \qquad [8]$$

where

$$I(g_{l,cr}) = \int_{g_{l,cr}}^{1} 180 \frac{(1-g_l)^2}{g_l^2} \frac{\mathrm{d}\theta}{\mathrm{d}g_l} \mathrm{d}g_l \qquad [9]$$

The integral $I(g_{l,cr})$ in Eq. [9] can be evaluated analytically if simplifying assumptions are made about the solid fraction-temperature curve, as in References 1, 6, 9, and 10. In the present study, however, this integral is evaluated numerically, using available alloy solid fraction-temperature curve data. The use of realistic solid fraction-temperature curve data makes the present criterion more general and accurate than previous criteria. This is especially true for industrially relevant multicomponent alloys for which analytical expressions for $\theta(g_l)$ cannot be obtained.

Introducing the Niyama criterion from Eq. [1] and rearranging Eq. [8] provides an expression for the present dimensionless Niyama criterion, Ny^*:

$$Ny^* = \frac{G\lambda_2\sqrt{\Delta P_{cr}}}{\sqrt{\mu_l \beta \Delta T_f \dot{T}}} = \frac{Ny}{\sqrt{\mu_l \beta \Delta T_f / \Delta P_{cr}}/\lambda_2} = \sqrt{I(g_{l,cr})} \qquad [10]$$

The dimensionless Niyama criterion given by Eq. [10] accounts not only for the local thermal conditions ($\dot{T}$, G) considered by the original Niyama criterion, but also for the properties and solidification characteristics of the alloy (μ_l, β, ΔT_f, and λ_2) and the critical pressure drop across the mushy zone (ΔP_{cr}). The most important feature of Eq. [10] is that Ny^* can be expressed as a function of only the solid fraction-temperature curve ($Ny^* = \sqrt{I(g_{l,cr})}$), whereas Ny is a function of the solid fraction-temperature curve, the SDAS, the critical pressure drop, and the other parameters in the denominator of the third term in Eq. [10]. It will be demonstrated later that this feature generalizes the predictive capability of this new criterion.

The SDAS can be determined as a function of the cooling rate from the relation

$$\lambda_2 = C_\lambda \dot{T}^{-1/3} \qquad [11]$$

where C_λ is taken as a material constant. Using Eq. [11], the following alternate form of Eq. [10] can be written

$$Ny^* = C_\lambda \frac{G}{\dot{T}^{5/6}} \sqrt{\frac{\Delta P_{cr}}{\mu_l \beta \Delta T_f}} = C_\lambda \dot{T}^{-1/3} Ny \sqrt{\frac{\Delta P_{cr}}{\mu_l \beta \Delta T_f}} \qquad [12]$$

Equation [12] indicates that the dimensionless Niyama criterion is proportional to $G/\dot{T}^{5/6}$, rather than to $G/\dot{T}^{1/2}$, as in the original Niyama criterion. This same functional dependence was also found in References 6, 9, and 10, in a slightly different form in each. The difference from the original Niyama criterion in the dependence on thermal conditions is due solely to the SDAS and the effect that this arm spacing has on the permeability in the mushy zone. The increased dependence on the cooling rate can be expected to make the dimensionless Niyama criterion more generally applicable for widely varying section thicknesses and different mold materials (sand, steel, copper, *etc.*).

Using the first equality in Eq. [10], the dimensionless Niyama criterion can be evaluated by casting simulation software in the same manner as the existing Niyama criterion. Once Ny^* is known, Eq. [10] also provides the value of the integral, $I(g_{l,cr})$. Knowledge of this value allows one to determine the critical liquid fraction at which porosity begins to form, $g_{l,cr}$, from Eq. [9]. Note that $g_{l,cr}$ appears only in the integration limit in Eq. [9]; thus, it cannot be directly determined from the equation. However, it will be illustrated in Section III that this value can be inversely determined from the value of $I(g_{l,cr})$. Once the critical liquid fraction has been determined, it is possible to use the continuity equation to approximate the final pore volume fraction, g_p. By assuming that local feeding flow ceases once shrinkage porosity forms (*i.e.*, the remaining shrinkage is fed by porosity formation only), the continuity equation can be simplified and integrated to give the relation

$$g_p = \beta' g_{l,cr} \qquad [13]$$

where $\beta' = \beta/(\beta+1) = (\rho_s - \rho_l)/\rho_s$. (Recall that $\beta = (\rho_s - \rho_l)/\rho_l$.)

The use of Eq. [13] to approximate the final pore volume fraction in conjunction with the dimensionless Niyama criterion is a novel concept that significantly enhances the usefulness of this new criterion. Rather than having to compare criterion values to generally unknown threshold values to determine whether porosity forms, the present criterion allows one simply to compute the volume fraction of shrinkage porosity throughout the casting. To summarize, the dimensionless Niyama criterion, Ny^*, can be calculated from local casting conditions and material properties using Eq. [10], which also provides the value of the integral $I(g_{l,cr})$. This integral value is then used to determine the value of $g_{l,cr}$ using Eq. [9]. Finally, Eq. [13] is used to determine the shrinkage pore volume fraction, g_p. When the new criterion is incorporated into casting simulation software, the user need not even be aware of it; the software can simply provide throughout the casting the volume fraction of shrinkage porosity predicted by the present method.

III. SHRINKAGE POROSITY PREDICTION

The dimensionless Niyama criterion developed in Section II is now used to develop pore volume fraction curves for several representative alloys, to investigate how changes in the critical pressure drop and the cooling rate affect the resulting pore volume, and to determine and analyze threshold values for porosity formation.

A. *Porosity Percentage Results*

Knowledge of the dimensionless Niyama criterion value, Ny^*, allows for the determination of the final pore

volume fraction (or percentage), g_p, *via* the relationship $Ny^* \rightarrow I(g_{l,cr}) \rightarrow g_{l,cr} \rightarrow g_p$, as explained in Section II. The only alloy-dependent quantities needed are the solid fraction-temperature curve and the total solidification shrinkage, β'. Dimensionless solid fraction-temperature curves are provided in Figure 3 (shown in terms of $g_l = 1 - g_s$), for three different alloys: WCB steel, aluminum alloy A356, and magnesium alloy AZ91D. The compositions of these alloys are provided in Table I. The freezing ranges, liquidus temperatures, and solidification shrinkage values for these alloys are provided in Table II. The WCB data set was generated using the interdendritic solidification simulation software IDS (Laboratory of Metallurgy, Helsinki University of Technology, Espoo, Finland), developed by Miettinen.[11] The A356 and AZ91D data sets were generated using a Scheil analysis within the thermodynamic software JMatPro (Sente Software Ltd., Surrey Technology Centre, Surrey, United Kingdom).[12] Using solid fraction-temperature curves such as those given in Figure 3, the integral in Eq. [9] can be evaluated numerically, using a spreadsheet. Figure 4 illustrates the resulting relationship between $I(g_{l,cr})$ and the critical liquid fraction, $g_{l,cr}$, for the three alloys considered in Figure 3. As mentioned earlier, Eq. [9] is used to determine the value of $g_{l,cr}$, which appears only in the integration limit. However, Figure 4 illustrates that there is a one-to-one correspondence between $I(g_{l,cr})$ and $g_{l,cr}$. Curves such as those given in Figure 4 can be generated for any alloy and stored in that alloy's material database. Then, during a simulation, the value of $g_{l,cr}$ can be easily determined by interpolation for any value of $I(g_{l,cr})$.

Using the results from Figure 4 in conjunction with Eq. [13], the pore volume fraction, g_p, can now be plotted directly as a function of the dimensionless Niyama criterion, Ny^*. This is depicted in Figure 5 for the WCB, A356, and AZ91D alloys considered here. Table III provides curve fits for each of these alloys, using the equation

$$g_p \text{ (pct)} = \min\left\{\beta'; \left(-A \log_{10}(Ny^*) + B + C(Ny^*)^{-D}\right)\right\} \quad [14]$$

Note that the maximum shrinkage porosity value is given by the total solidification shrinkage (*i.e.*, $g_{p,\max} = \beta'$). Figure 5 demonstrates that decreasing the dimensionless Niyama criterion below a certain threshold value results in an increase in the final pore volume percentage. It is important to note that Figure 5 is a semilog plot, which is necessitated by the large range of Ny^* values that are possible. While the variation in g_p

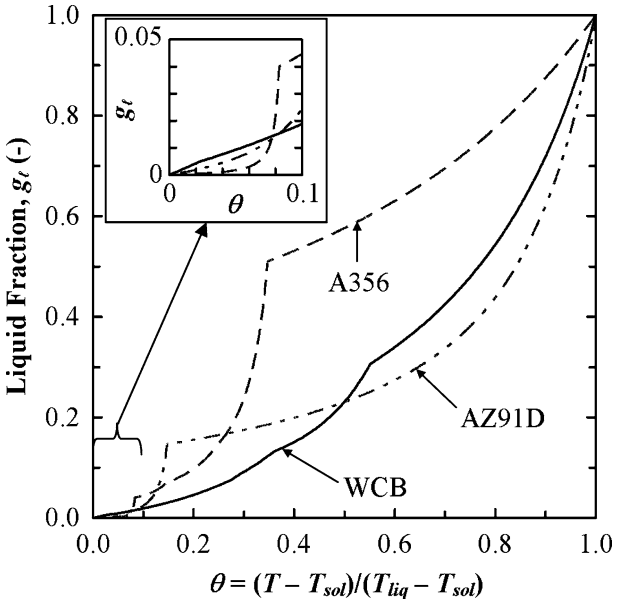

Fig. 3—Liquid fraction as a function of dimensionless temperature, θ, for WCB steel, aluminum alloy A356, and magnesium alloy AZ91D.

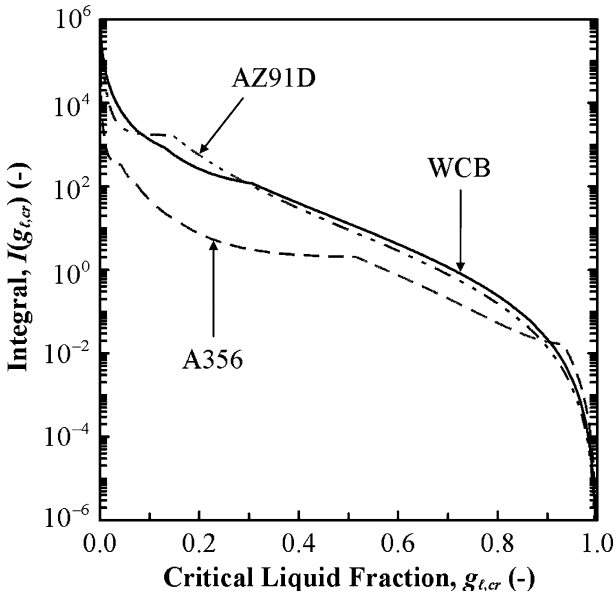

Fig. 4—Variation in the integral from the dimensionless Niyama criterion derivation, with critical liquid fraction.

Table II. Parameters Used in the Dimensionless Niyama Criterion and Shrinkage Porosity Calculations

Alloy	Dynamic Viscosity, μ_l (mPa s)	Solidification Contractions, β, β' (Pct)	Freezing Range, ΔT_f (°C)	Liquidus Temperature, T_{liq} (°C)	Critical Pressure Drop, ΔP_{cr} (Bar)	Constant C_λ in Eq. [11] (μm (°C/s)$^{1/3}$)
WCB	5.63	4.49, 4.30	70.8	1509	1.01	144
A356	1.58	5.89, 5.57	65.3	616	1.01	40.9
AZ91D	1.58	5.69, 5.38	200	603	1.01	35.5

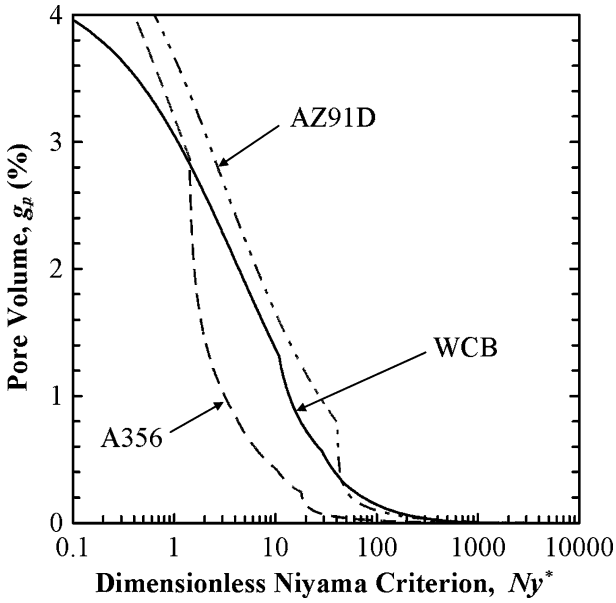

Fig. 5—Predicted pore volume as a function of dimensionless Niyama criterion for WCB steel, A356, and AZ91D.

with Ny^* is qualitatively similar for all alloys, the semilog nature of the plot disguises the fact that there can be considerable differences among the alloys in the Ny^* values corresponding to a given porosity percentage. For example, for A356, a value of $g_p = 1$ pct is obtained for $Ny^* \approx 3$, whereas for AZ91D, this porosity level is reached at $Ny^* \approx 30$. Of particular interest in Figure 5 is the region of Ny^* values in which the pore volume asymptotically approaches zero. Again, due to the scale used in Figure 5, the details of this transition to a shrinkage-free state are not readily apparent for each alloy. The issue of threshold Niyama values, above which the shrinkage pore volume fraction is below a certain specified level, is discussed separately in Section III–C.

B. *Parametric Studies*

The first parametric study investigates the effect of the critical pressure drop, $\Delta P_{cr} = P_{\text{liq}} + P_\sigma$, on the resulting pore volume. Recall from the discussion in Section II that the critical mushy zone pressure drop that corresponds to the beginning of pore formation is generally an unknown parameter. The alloy selected for this parametric study was WCB steel (Table II). Calculations were performed for a cooling rate of $\dot{T} = 1\,^\circ\text{C/s}$ and a temperature gradient of $G = 100\,^\circ\text{C/m}$, which gives a constant Niyama value from Eq. [1] of $Ny = 0.1\ (^\circ\text{C s})^{1/2}/\text{mm}$. The critical pressure drop was varied from one simulation to the next, and the corresponding dimensionless Niyama value for each critical pressure drop was computed using Eq. [10]. Then, using the data from Figure 5, the pore volume percentage was determined for each dimensionless Niyama value. The resulting relationship between the critical pressure drop and the shrinkage porosity is given in Figure 6, in which the critical pressure drop varies from 1 to 21 bar. Assuming that the melt pressure at the liquidus temperature is equal to atmospheric pressure ($P_{\text{liq}} = 1.01$ bar), the pressure range in Figure 6 corresponds to a capillary pressure variation from 0 to 20 bar. The symbol on the left end of the curve in this figure denotes the limiting case of zero capillary pressure. Figure 6 shows that the pore volume fraction decreases rapidly as the critical pressure drop increases from 1.01 bar (zero capillary pressure); the decrease, however, becomes more gradual after approximately 6 bar. Capillary pressures much above 5 bar are clearly not realistic; for steel (with $\sigma \approx 0.86$ N/m), $P_\sigma = 5$ bar corresponds to an initial pore radius of curvature of only $r_0 = 3.4\ \mu$m. One could also interpret Figure 6 in terms of the effect of varying the ambient pressure, *i.e.*, varying P_{liq} for a constant P_σ. From this viewpoint, it is evident that increasing the ambient pressure (by casting pressurization, for example) decreases the shrinkage porosity. Pressurization values up to 5 bar significantly reduce the pore volume, but pressurization begins to have a diminishing return in shrinkage porosity reduction beyond approximately 5 bar.

The second parametric study investigates the effect of variations in the cooling rate on the resulting pore volume for WCB steel. Recall from Section II that the dimensionless Niyama criterion is proportional to $G/\dot{T}^{5/6}$ rather than to $G/\dot{T}^{1/2}$, as in the original Niyama criterion. It is of interest to explore the effect of this difference on the predicted shrinkage porosity. For this parametric study, the cooling rate was varied, but the Niyama value was

Table III. Shrinkage Porosity Curve Fit Data for WCB, AZ91D, and A356

$$g_p\ (\text{pct}) = \min\left\{\beta';\left(-A\log_{10}(Ny^*) + B + C(Ny^*)^{-D}\right)\right\}$$

Alloy	Ny^* range	A	B	C	D
WCB	$Ny^* \le 28.2$	1.654	3.052	0	0
	$Ny^* > 28.2$	0	0	43.05	1.254
AZ91D	$Ny^* \le 41.0$	1.671	3.483	0	0
	$41.0 < Ny^* \le 45.2$	10.81	18.23	0	0
	$Ny^* > 45.2$	0	0	73.01	1.415
A356	$Ny^* \le 1.43$	2.068	3.160	0	0
	$1.43 < Ny^* \le 18.0$	0	0	4.024	0.9786
	$Ny^* > 18.0$	0	0	7.771	1.206

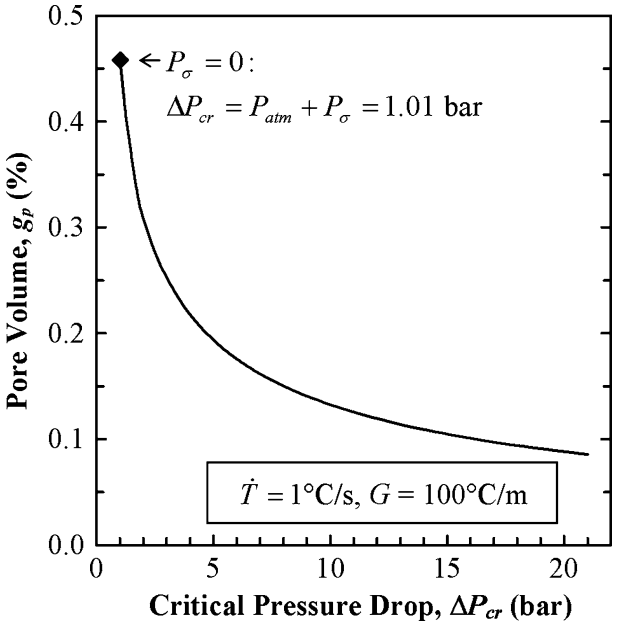

Fig. 6—Effect of critical pressure drop on final pore volume in WCB steel. The diamond represents the limiting case with zero capillary pressure.

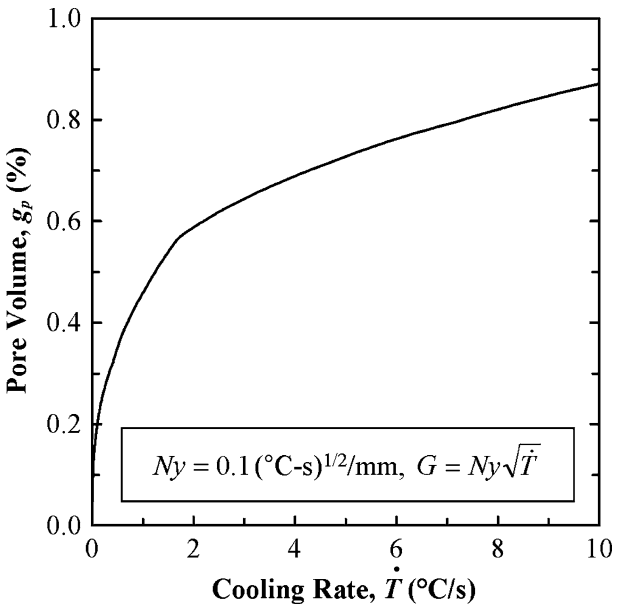

Fig. 7—Variation in pore volume in WCB steel with cooling rate, for a constant Niyama criterion value.

held constant at $Ny = 0.1$ (°C s)$^{1/2}$/mm by calculating the temperature gradient for each cooling rate from Eq. [1] as $G = Ny\sqrt{\dot{T}}$. A critical pressure drop of $\Delta P_{cr} = 1.01$ bar was used for all simulations. For each cooling rate, the dimensionless Niyama value was computed using Eq. [12]; data from Figure 5 were then used to determine the pore volume. Figure 7 displays the variation in the pore volume percentage with cooling rate at a constant Niyama value, for cooling rates ranging from 0 to 10 °C/s. The pore volume is nearly zero for very small cooling rates. It increases rapidly as the cooling rate begins to increase from zero; then the increase becomes more gradual above approximately 2 °C/s. Because the Niyama value is being held constant, the third term in Eq. [10] indicates that the variation in pore volume seen in this figure is due entirely to differences in the SDAS and to the effect that the SDAS has on the permeability in the mushy zone. For very small cooling rates, the arm spacing is large, which leads to a large permeability and low porosity. As the cooling rate increases, the arm spacing and, subsequently, the permeability decrease, leading to an increase in pore volume. Figure 7 highlights one of the benefits gained from generalizing the Niyama criterion; although the original Niyama criterion accounts for the thermal conditions, it does not account for the effect of the thermal conditions on the SDAS, which can significantly affect the resulting pore volume.

C. *Threshold Criterion Values*

Figure 5 illustrates that the shrinkage porosity becomes negligible for large values of Ny^*. This phenomenon can be quantified by defining threshold dimensionless Niyama values that correspond to specified final shrinkage porosity levels. The threshold values considered here correspond to final porosity levels of 0.1 pct ($Ny^*_{0.1\text{pct}}$) and 0.01 pct ($Ny^*_{0.01\text{pct}}$). For example, if $Ny^* > Ny^*_{0.1\text{pct}}$, the resulting shrinkage porosity will be less than 0.1 pct. Threshold dimensionless Niyama values are given for the alloys WCB, A356, and AZ91D in Table IV. Note that these threshold values are only a function of the solid fraction-temperature curve and the solidification shrinkage of the alloy. The threshold values for the WCB and AZ91D are comparable, and the values for A356 are significantly lower than for the other alloys. This can also be seen in Figure 5 where, as Ny^* increases, the A356 curve drops to low porosity values much sooner than in the other alloys. The nature of the dimensionless threshold values can be traced to the shape of the "tail" (*i.e.*, the region containing the last ~10 pct of liquid) of the solid fraction-temperature curves of these alloys, as shown in the inset in Figure 3. The tail of the WCB and AZ91D curves in this figure are similar, while the tail of the A356 curve drops down more rapidly as the solid fraction decreases. Clearly, without using realistic solid fraction-temperature curves for these alloys, these differences could not be predicted.

Table IV also includes corresponding threshold values for the original Niyama criterion, $Ny_{0.1\text{pct}}$ and $Ny_{0.01\text{pct}}$. These threshold values were computed from the threshold dimensionless values using Eq. [12], with the parameters listed in Table II. The original Niyama threshold values are a function of the cooling rate as well as of the alloy, due to the SDAS effect mentioned earlier. Table IV lists original Niyama threshold values for a range of cooling rates and includes the SDAS for each cooling rate for the given alloy. Although it is not investigated in Table IV, the original Niyama threshold values are also a function of the critical pressure drop, as mentioned in the discussion of Figure 6. Due to the uncertainty in the capillary pressure, the same limiting

Table IV. Threshold Porosity Values for Dimensionless Niyama Criterion and Niyama Criterion

Alloy	$Ny^*_{0.01\text{pct}}$	$Ny^*_{0.1\text{pct}}$	Cooling Rate, $\dot{T}$ (°C/s)	SDAS, λ_2 (μm)	$Ny_{0.01\text{pct}}$ ((°C s)$^{1/2}$/mm)	$Ny_{0.1\text{pct}}$ ((°C s)$^{1/2}$/mm)
WCB	610	137	10	67.0	3.83	0.86
			1	144	1.78	0.40
			0.1	311	0.83	0.19
A356	211	23	10	19.0	2.72	0.30
			1	40.9	1.26	0.14
			0.1	88.0	0.59	0.065
AZ91D	776	99	10	16.5	19.8	2.53
			1	35.5	9.19	1.17
			0.1	76.6	4.26	0.54

value of ΔP_{cr} = 1.01 bar was used for all three alloys. This value can be interpreted as corresponding to a casting at atmospheric pressure and a vanishing capillary pressure at pore formation (P_σ = 0 bar), which represents a worst-case (*i.e.*, maximum shrinkage porosity) scenario. If original Niyama threshold values are desired for a different ΔP_{cr}, the threshold values given in Table IV can simply be multiplied by $\sqrt{1.01 \text{ bar}/\Delta P_{cr}}$ (Eq. [12]).

For all three alloys, the original Niyama criterion threshold values in Table IV are dependent on the cooling rate: each decrease by a factor of 10 in the cooling rate causes corresponding threshold values to decrease by approximately a factor of 2. This is an important point to consider when using the original Niyama criterion to predict porosity in a casting. When interpreting original Niyama results from a casting simulation, foundry engineers typically use a single, constant value as the threshold for shrinkage porosity formation. Table IV shows that, in reality, the threshold depends on the cooling rate. Table IV also indicates how original Niyama threshold values change with the metal alloy. Considering the $Ny_{0.1\text{pct}}$ threshold values for $\dot{T}$ = 1 °C/s, one sees that the threshold value for A356 aluminum is 3 times smaller than the value for WCB steel, and the value for AZ91D is 3 times larger than that for WCB. While it is true that threshold values also change with the alloy for the dimensionless Niyama criterion, these dimensionless threshold values can be predicted from knowledge of the solid fraction-temperature curve and the solidification shrinkage only; the threshold values for the original Niyama criterion, however, must be determined empirically for each alloy. Furthermore, although the dimensionless Niyama threshold values are included in Table IV for completeness, they are not important. Threshold Ny^* values are unnecessary in practice, because one can simply compute the pore volume percentage corresponding to a given value of Ny^*.

In order to examine the validity of the Niyama threshold values listed in Table IV, the values can be compared to those found experimentally by the present authors in previous work involving WCB steel sand castings. The Niyama threshold value found previously for centerline macroshrinkage (shrinkage visible on standard production film radiographs) in plate castings, such as the one depicted in Figure 1, was equal to 0.1 (°C s)$^{1/2}$/mm.[2] This value compares well with the $Ny_{0.1\text{pct}}$ values given for WCB steel in Table IV, particularly the value of 0.19 (°C s)$^{1/2}$/mm for $\dot{T}$ = 0.1 °C/s. The cooling rate in the plate castings of the experimental study was approximately 0.1 °C/s (at the centerline) to 1 °C/s (at the surface); therefore, this is a reasonable comparison. Similarly, the threshold Niyama value found previously in another study by the present authors for microshrinkage (not visible on radiographs) sufficient to cause leaks in various complex-shaped steel castings was approximately 1.0 (°C s)$^{1/2}$/mm.[3] This value compares well with the $Ny_{0.01\text{pct}}$ threshold values for steel in Table IV, particularly the values of 0.83 and 1.78 (°C s)$^{1/2}$/mm for $\dot{T}$ = 0.1 and 1.0 °C/s, respectively. These comparisons indicate that the $Ny_{0.1\text{ pct}}$ (and $Ny^*_{0.1\text{pct}}$) values in Table IV may be reasonable threshold values for macroshrinkage, while the $Ny_{0.01\text{ pct}}$ (and $Ny^*_{0.01\text{pct}}$) values in Table IV may be appropriate threshold values for microshrinkage. More exact comparisons are not possible, because actual porosity volumes were not measured in the experiments.

Finally, it should be mentioned that the threshold value found in the original study by Niyama *et al.*[1] involving steel sand castings is equal to 1 (°C min)$^{1/2}$/cm = 0.775 (°C s)$^{1/2}$/mm. This study also relied on film radiographs of limited sensitivity to detect the presence of shrinkage porosity. It can be seen that the threshold value proposed by Niyama *et al.* is comparable to the original Niyama threshold values listed in Table IV for cooling rates between 0.1 and 1.0 °C/s, which are typical for steel sand castings.

IV. APPLICATION TO 3-D CASTINGS

The present method for predicting the shrinkage pore volume percentage from the dimensionless Niyama criterion was implemented in the general-purpose casting simulation software package MAGMASOFT*,[13] in order to allow calculations to be performed for complex-shaped castings. Original Niyama criterion values are provided by MAGMASOFT as part of the normal simulation output. The application programming interface

*MAGMASOFT is a registered trademark of MAGMAGmbH, Aachen, Germany.

(API) in MAGMASOFT was then used to postprocess the existing results, in order to calculate Ny^* from Eq. [10] and then calculate g_p using the equations given in Table III. The temperature gradient and cooling rate values required to calculate Ny and Ny^* were evaluated at a temperature 10 pct of ΔT_f above T_{sol}. This evaluation point was selected because it is late in solidification, when shrinkage porosity is likely to be forming.

A. *WCB Steel Plate Castings*

The first 3-D simulation performed was for the WCB steel plate shown in Figure 1. As discussed in Section I, 15 such plates were cast and analyzed, giving the composite through-thickness porosity plot shown in Figure 1(d). The solidification of these 15 plates was simulated using the available casting data.[2] Only the solidification was simulated (no filling); therefore, the gating was not included. The initial steel temperature was taken as 1569 °C, which corresponds to a superheat of 60 °C. The present WCB property data set, generated using IDS, including the parameters listed in Table II, was used in the simulation. The sand mold was modeled using the MAGMASOFT database FURAN. Finally, the mold-metal interfacial heat transfer coefficient was taken as a constant value of 1000 W/m^2 K.

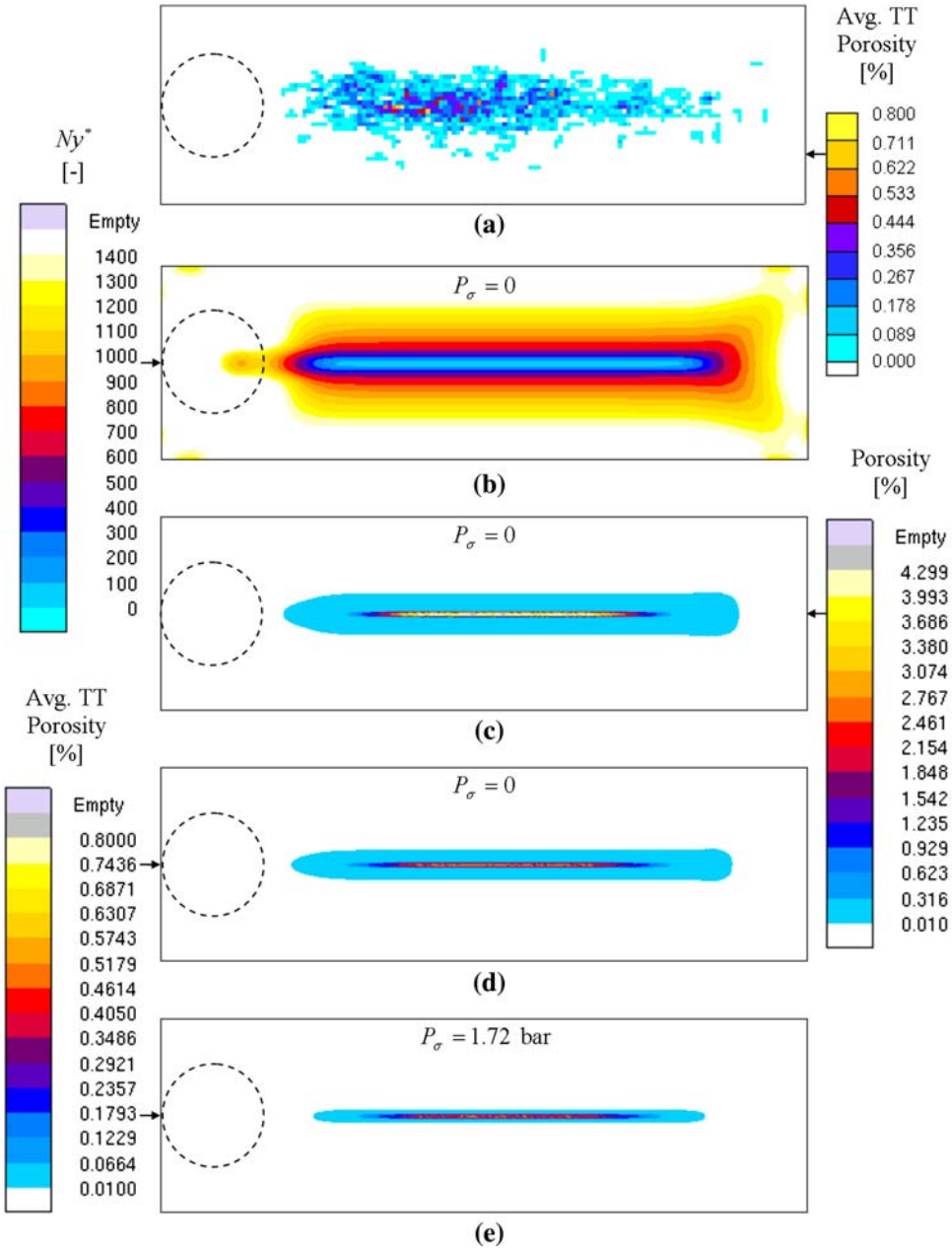

Fig. 8—Comparison between experimental shrinkage porosity and dimensionless Niyama criterion predictions for WCB steel plates: (*a*) average through-thickness porosity of 15 WCB steel plates; (*b*) and (*c*) midplate views of the dimensionless Niyama criterion distribution and the shrinkage porosity distribution for these plates, respectively; and (*d*) and (*e*) predicted through-thickness porosity distribution for these plates.

The results of these calculations are shown in Figure 8. For comparison, the experimental through-thickness porosity result from Figure 1(d) is repeated in Figure 8(a). The dimensionless Niyama criterion contours for the midthickness plane of the plate are shown in Figure 8(b). Comparing this result to the original Niyama criterion contours shown in Figure 1(e), it is seen that the low Ny values at the plate centerline lead to low Ny^* values in the same region in Figure 8(b). The predicted midplane shrinkage pore volume percentages, g_p, corresponding to these Ny^* values are shown in Figure 8(c). No values are shown below 0.01 pct. The maximum value found at the centerline, 4.3 pct, is simply β'. In order to allow for a direct comparison with the radiography results in Figure 8(a), the predicted porosity distribution was averaged through the thickness of the plate by means of the MAGMASOFT API (recall that Figure 8(c) shows the calculated porosity only at the midthickness plane). Figure 8(d) shows the calculated average through-thickness porosity contours, using a scale similar to the one in the experimental plot in Figure 8(a), with the same maximum porosity value (0.8 pct). The measured and predicted results are in good agreement, both in terms of the spatial extent of the shrinkage-containing region and the actual porosity percentages. It should be kept in mind, however, that this comparison is not fully quantitative, because the porosity observed on the radiographs was assumed to be always 1 mm in depth (Section I), which can only be viewed as a first approximation. Nonetheless, the good agreement is remarkable, considering that the porosity prediction is based solely on a criteria function.

Finally, Figure 8(e) shows the average through-thickness porosity distribution obtained for a critical pressure drop of $\Delta P_{cr} = 2.73$ bar, instead of the $\Delta P_{cr} = 1.01$ bar used in the simulation for Figure 8(d). With the casting at atmospheric pressure, the higher critical pressure drop can be interpreted as corresponding to a capillary pressure of $P_\sigma = 1.72$ bar at pore formation, which in turn implies an initial pore radius of curvature of approximately $r_0 = 10$ μm. It can be seen that the predicted porosity distributions are quite similar for the two critical pressure drops; the main difference is in the extent of the low-porosity region surrounding the narrow centerline indications. The maximum centerline values are the same in both cases, because the porosity volume fraction cannot exceed β'. Comparing both predictions with the experimental results in Figure 8(a), it appears that the extent of shrinkage porosity is better predicted by the simulation with $\Delta P_{cr} = 1.01$ bar, which represents the most conservative case possible. Nonetheless, the similarity of the two results suggests that capillary pressures on the order of 1 to 2 bar are still realistic.

B. *AZ91D Magnesium Alloy Plate Castings*

In addition to the WCB plate simulation, two additional solidification simulations were performed for the same plate geometry using the magnesium alloy AZ91D. Both simulations used a superheat of 60 °C. One of these simulations used a sand mold (MAGMASOFT FURAN database) and the other used a steel mold (MAGMASOFT STEEL database). The interfacial heat transfer coefficient was taken as a constant value of 1000 W/m^2 K for the sand mold simulation and as a constant value of 2500 W/m^2 K for the steel mold simulation. The simulated cooling rates at the plate midplane that resulted from these two types of molds were quite different: for the sand mold, the cooling rates varied from approximately 0.1 °C/s to 0.3 °C/s; for the steel mold, the cooling rates varied from approximately 5 °C/s to 10 °C/s. The shrinkage porosity calculations used the AZ91D data given in Table II. No experimental shrinkage data are available for comparison, but the results are interesting, nonetheless.

Figure 9 provides plate midthickness-plane results from these simulations. Original Niyama contour plots are shown in Figures 9(a) (sand mold) and (b) (steel mold); pore volume contour plots are shown in Figures 9(c) (sand mold) and (d) (steel mold). Comparing the AZ91D Niyama contour plots to the corresponding WCB steel plot in Figure 1(e), one sees a great difference in the nature of the Niyama distributions. For the WCB steel, the low-Niyama regions (colored regions) are confined to the center of the plate. For the AZ91D, using both sand and permanent molds, low-Niyama regions exist throughout the plates. The cooling rates for the WCB and AZ91D sand castings are comparable, which implies that the substantial difference in Niyama contours is due to differences in the thermal gradients (Eq. [1]). The thermal gradients in AZ91D castings during solidification are substantially shallower than those for comparable WCB castings, due to differences in the thermal conductivity and heat capacity of the two alloys. From Eq. [1], it is evident that smaller gradients will yield lower Niyama values. Comparing the sand and permanent mold Niyama results for AZ91D in Figures 9(a) and (b), the differences due to different cooling rates can be seen. The permanent mold has lower Niyama values in the center of the plate, due to higher cooling rates (Eq. [1]). However, the permanent mold result has higher Niyama values near the plate edges. This is due to a combination of the changes in both the cooling rates and the temperature gradients in these regions.

When comparing the predicted porosity fields for the two AZ91D simulations, one sees that the steel mold result (Figure 8(d)) shows a much larger amount of shrinkage porosity than the sand-casting result (Figure 8(c)). If one considers the Niyama values in the center of the plate to be comparable, this result is consistent with Figure 7: for comparable Niyama values, higher cooling rates lead to higher pore volumes due to smaller SDAS values and, hence, lower permeability in the mushy zone. It is interesting to find less shrinkage porosity in AZ91D sand castings compared to steel mold castings, but these results have yet to be verified experimentally. Finally, viewing the Niyama plots in Figures 9(a) and (b) and then comparing these fields to the pore volume plots in Figures 9(c) and (d), it should be noted that it would be nearly impossible to guess the extent of the porosity in each case based solely on these Niyama plots. This result highlights the cooling rate

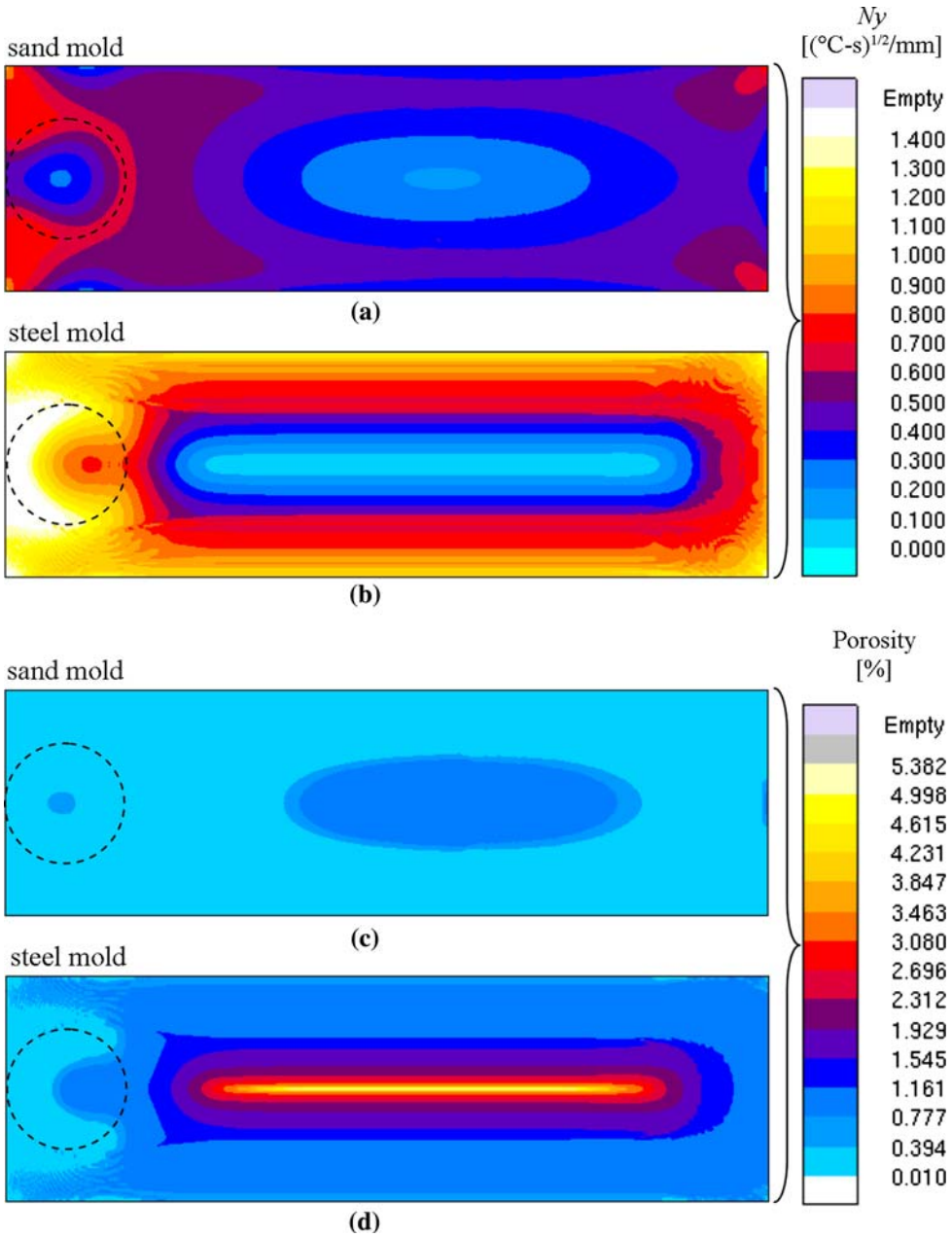

Fig. 9—Simulated Niyama criterion and shrinkage porosity contour results for an AZ91D plate casting. Results (*a*) and (*c*) are for a furan sand mold; results (*b*) and (*d*) are for a steel mold.

dependence in Niyama threshold values for predicting shrinkage porosity. It also emphasizes the benefit of directly predicting pore volumes using the present method instead of requiring a user to interpret criteria plots in terms of threshold values.

V. CONCLUSIONS

A generalized, dimensionless form of the Niyama criterion (Ny^*) has been developed, along with a method to use this criterion to directly predict shrinkage pore volume fractions in casting solidification. The new criterion, which can be calculated by any casting simulation software in the same manner as the original Niyama criterion (Ny), accounts not only for thermal conditions during casting (as in the original criterion), but also for alloy material properties, solidification characteristics, and the critical pressure for pore formation. The additional parameters taken into account by Ny^* make it more generally applicable for casting shrinkage prediction. This study demonstrates how the shrinkage pore volume fraction can be directly related to Ny^* for any alloy, knowing only the solid fraction-temperature curve and the total solidification shrinkage of the alloy. Parametric studies are used to illustrate the effect of the critical pressure drop and the cooling rate on the final pore volume.

Threshold Niyama values, above which the shrinkage porosity is limited to a specified small value, are predicted for three representative foundry alloys. The WCB steel threshold values are in good agreement with previous experimental observations. Finally, the new method developed in the present study is used in conjunction with a casting simulation software package to predict shrinkage porosity in 3-D castings. Comparisons between simulated and experimental shrinkage porosity results for a WCB steel plate sand casting demonstrate that the method can reasonably predict shrinkage. Additional simulations for the magnesium alloy AZ91D illustrate that the new method is applicable to alloys other than steel. Experimental validation for this and for other alloys is certainly warranted. It is important to note that, because this method is based on Darcy's law, it predicts only feeding-related shrinkage porosity caused by shallow temperature gradients. It predicts neither gas porosity nor shrinkage that forms in isolated pools of liquid in a solidifying casting.

REFERENCES

1. E. Niyama, T. Uchida, M. Morikawa, and S. Saito: *AFS Cast Met. Res. J.*, 1982, vol. 7, pp. 52–63.
2. K.D. Carlson, S. Ou, R.A. Hardin, and C. Beckermann: *Metall. Mater. Trans. B*, 2002, vol. 33B, pp. 731–40.
3. K. Carlson, S. Ou, R. Hardin, and C. Beckermann: *2001 SFSA Technical and Operating Conf*, SFSA, Crystal Lake, IL, 2001.
4. K.D. Carlson, S. Ou, and C. Beckermann: *Metall. Mater. Trans. B*, 2005, vol. 36B, pp. 843–56.
5. F. Chiesa, B. Duchesne, G. Bournival, and G. Morin: *Am. Foundrymen's Soc. Trans.*, 2006, vol. 114, pp. 667–81.
6. G.K. Sigworth and C. Wang: *Metall. Trans. B*, 1993, vol. 24B, pp. 349–64.
7. K.D. Carlson, Z. Lin, and C. Beckermann: *Metall. Mater. Trans. B*, 2007, vol. 38B, pp. 541–55.
8. S. Ou, K.D. Carlson, and C. Beckermann: *Metall. Mater. Trans. B*, 2005, vol. 36B, pp. 97–116.
9. Y.W. Lee, E. Chang, and C.F. Chieu: *Metall. Trans. B*, 1990, vol. 21B, pp. 715–22.
10. J. Dantzig and M. Rappaz: *Solidification*, 1st ed., EPFL Press, Lausanne, Switzerland, in press.
11. J. Miettinen: *Metall. Mater. Trans. B*, 1997, vol. 28B, pp. 281–97.
12. JMatPro v.4.0, Sente Software Ltd., Surrey Technology Centre, Surrey GU2 7YG, United Kingdom.
13. MAGMASOFT v4.5, MAGMA GmbH, Aachen, Germany.